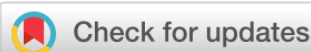


Original Research

View Article Online



Received 03 February 2024

Revised 27 May 2024

Accepted 29 May 2024

Available online 13 July 2024

Edited by Balamuralikrishnan Balasubramanian

KEYWORDS:

AgO/Fe₂O₃-NCs

PLA (Nd-YAG)

Marine shrimp shell

Caridean

Anti-microbial activity

Natr Resour Human Health 2024; 4 (3): 318-327

<https://doi.org/10.53365/nrfhh/189493>

eISSN: 2583-1194

Copyright © 2024 Visagaa Publishing House

Development of a neutral resource for nano-AgO/Fe₂O₃ composite preparation by mixing marine shrimp shell extract with metal salts for anti-microbial activity

Duha A. Kadhim^{1,*}, Abdul Haleem A. Raheem¹, Nada Qasim¹, Muslim A. Abid¹, Ihab Adnan Thabet¹

¹Department of Physics, College of Science, Mustansiriyah University, Baghdad, Iraq

ABSTRACT: Marine shrimp shell, a member of the Caridean biological family, is an aquatic crustacean used in aquariums with a wide range of pharmacological activities. This study's success in the development of a natural resource of silver oxide/iron oxide nanocomposite (NCs) (AgO/Fe₂O₃ NCs) prepared by combining a marine shrimp shell extract with Ag₂NO₃ and FeCl₃ salt via a PLA (Nd-YAG) process. AgO/Fe₂O₃ NCs are vital to antibacterial because they kill germs and maintain a disease-free environment. XRD analysis, FE-SEM pictures, TEM images, EDS, mapping, and FTIR spectra were employed to investigate AgO/Fe₂O₃ NCs. The XRD data indicates that AgO/Fe₂O₃ NCs have a face centre cubic F.C.C. structure with a range of crystallite sizes between 9.6 and 19.5 nm. Moreover, according to the FE-SEM data, the AgO/Fe₂O₃ NCs' average diameters of 10 to 20 nm revealed a nano-spherical shape. According to TEM scans, AgO/Fe₂O₃ NCs varied in size from 15.4 to 23 nm and were spherical with aggregation in form. Ag, Fe, and O occurrences were present in high-purity AgO/Fe₂O₃ NCs, as demonstrated by the EDS spectra with their picture. In the FTIR spectra, peaks related to the symmetric stretching vibrations of Ag-O and I-O bonds can be seen at 726 cm⁻¹. The inhibition zones of antibacterial AgO/Fe₂O₃ NCs were evaluated using diffusion. The inhibition zones measured 29 to 13.5 mm for gram-positive bacteria (*Staphylococcus aureus* and *Staphylococcus epidermidis*) and 40 mm for gram-negative bacteria (*Escherichia coli*); at *Candida*, the inhibition zone diameters (IZDs) value was 42 mm. To the best of the author's knowledge, combining marine shrimp shell extract with Ag₂NO₃ and FeCl₃ salt using a PLA (Nd-YAG) approach is novel and hasn't been discussed in any research publications yet.

1. INTRODUCTION

In comparison to traditional physical and chemical approaches, the development of natural resources for human health through the synthesis of nanoparticles (NPs) utilizing materials from animals (peels, fish, blood, bones, etc.) results in advancements in the production of low-cost, environmentally friendly, and long-lasting stabilized NPs. Massive population growth and a quick biological revolution have become significant environmental contamination characteristics. When used in medication, pesticides and insecticides might readily float into water or be transported by the wind, producing several hazardous substances that could harm human health and the environment (Luceri et al., 2023; Mercan et al., 2022; Sharmin et al., 2021). On the other hand, pathogenic microbes participate in releasing highly toxic pollutants, such as

Escherichia coli, *Staphylococcus aureus*, *Staphylococcus epidermidis*, and *Candida*. As a result, early monitoring and detection of these dangerous bacteria has emerged as a critical strategy for success. Nanoparticles are an essential component of this technology that provides workable solutions (W.S. Khan et al., 2016). Three categories comprise the different types of nanoparticles: metal oxide, nanocomposite, and nano-metal I. Khan et al. (2019). Although there are several applications for nanomaterials, little study has been done on nanocomposite, particularly concerning harmful bacteria (Prabhu & Poulouse, 2012). Both positive and negative bacteria severely threaten human health and the environment. When extreme toxicity is introduced into human systems in large concentrations, it can be fatal. It is essential to develop nanoparticles that can rapidly eradicate this bacterium for human health and environmental preservation (Prabhu &

* Corresponding author.

E-mail address: duha.abdual@uomustansiriyah.edu.iq (Duha A. Kadhim)

This is an open access article under the CC BY-NC-ND license (<http://creativecommons.org/licenses/by-nc-nd/4.0/>).

Poulose, 2012). The toxic substances secreted by bacteria and fungi are endotoxins and aflatoxin, and their pollutants affect the airways, mouth, digestive, reproductive, and urinary tracts, as well as the contamination of food and feed with mycotoxins.

In the last few decades, metal oxides like AgO, SnO₂, ZnO, Fe₂O₃, CuO, and beyond (Galúcio et al., 2022). Marine shrimp is a popular marine variety and a good source of protein. While marine shrimp contains few calories, it contains many essential nutrients. These nutrients include selenium, a mineral that shields cells from damage, and vitamin B12, which helps create red blood cells and maintains the neurological system's normal operation (USDA, 2020; USEPA, n.d.). Because of their intriguing physicochemical properties, iron oxide nanoparticles (IO-NPs) have also gained traction in research areas looking into anticancer, antifungal, plant growth, and antibacterial applications (Yamada et al., 1998). Because plant-based nanoparticles are more stable and economical than those derived from microbes, their biological production has potential value (Betty et al., 2022). Because of its regulated size, strong magnetic, and low toxicity, IO-NPs' nanoparticle activity is quite significant (Nasiri, 2023). To the best of the author's knowledge, the reason for this sort of work was the shortage of reports and studies about the use of PLA (Nd-YAG) procedures during the research on animal extracts. The primary objective of this work is to compare the AgO/Fe₂O₃-NCs utilizing the PLA (Nd-YAG) approach. The PLA (Nd-YAG) process can lead to higher purity, a suitable crystalline structure, non-toxicity, safety, affordability, and environmental friendliness.

Marine shrimp are low in fat and abundant in minerals and proteins, making them beneficial for health. Furthermore, two essential biological properties of thin products are the chemopreventive and chemoprotective properties of its lipids. Several biological activities of methanolic and lipidic extracts of shrimp waste and muscle have been reported. Through techniques gathered under the term "chemoprevention," which refers to using natural or synthetic compounds to prevent cancer and microbial formation, these actions, which can influence biological processes, have been related to cancer prevention (López-Saiz et al., 2013). One kind of shrimp that works well with particle structure is the white shrimp.

The previous studies in 2024 on iron oxide NP synthesis via a chemical method on bacterial cells (gram-positive and gram-negative) by Rishikesh Kumar et al. (Kumar et al., 2024). In 2024, metal and metal oxide nanoparticles will be synthesized using green synthesis for medical applications. Study effect size, shape, and distribution of NPs in their toxicity by de Jesus, R. A., et al. (De Jesus et al., 2024).

In this work, the AgO/Fe₂O₃-NCs preparation involves mixing the marine shrimp shell extract with Ag₂NO₃ and FeCl₃ salt for the first time via a PLA (Nd-YAG) method at 300 °C for 2 hours for antimicrobial activity. AgO/Fe₂O₃-NCs were characterized using XRD analysis (XRD-6000/Japan), and the JCPDS card (Joint Committee on Powder Diffraction Standards) was used to compare the findings. XRD measurements in the Nanotechnology Laboratory and Advanced Materials/The

Materials Research Department/The Ministry of Science and Technology in Iraq have been used to examine the orientation of AgO/Fe₂O₃-NCs developed samples. AgO/Fe₂O₃-NCs shape and particle size were analyzed using FE-SEM, TEM, and EDS-Mapping, tested in Iran-Mashhad at "Tescan Mira3 SEM-Czechia." The absorption peaks, the compound, and the functional group were determined via the FTIR spectrum (Perkin-Elmer Spectrum GX FTIR).

2. EXPERIMENTAL PART

2.1. Material and Methods

Table 1 displays the specs of the materials utilized in this project.

Table 1

The characteristics of the materials used in the study.

Material	Molecular equation	Companies	purity
Ferric salt	FeCl ₃	Merck-Millipore	99%
Silver nitrate	Ag ₂ NO ₃	Scharlau Spain	98%

2.2. Preparation of the marine shrimp shell extract

The biological name of the marine shrimp shell is Caridean (Islam et al., 2024). The local market in Baghdad, Iraq, provided the shells of marine shrimp. Marine shrimp shell samples taken for this investigation were taken to remove contaminants, sliced into little pieces, and then dried for nine days in an Umbra case. The dehydrated samples were then ground into a fine powder in a professional blender made of stainless steel. 200 ml of deionized water and 10 g of powdered mixture were used to create animal extracts. A magnetic stirrer brought The solution to a boil at 80 °C for two hours. The solution was frozen at room temperature and filtered through a Whatman filter sheet. Figure 1 (A–C) shows the stages of making the marine shrimp shell extract.

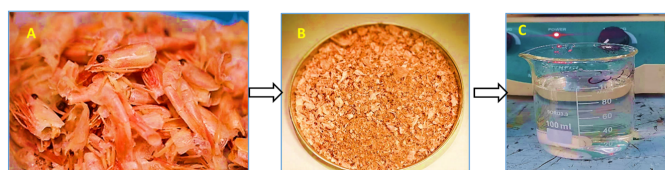


Figure 1. The synthesis stages for marine shrimp shell extract, A) the marine shrimp shell, B) the marine shrimp shell powder, and C) the marine shrimp shell extract.

2.3. Preparation of AgO/Fe₂O₃ NCs from marine shrimp shell extract by PLA (Nd-YAG technique)

To prepare AgO/Fe₂O₃-NCs, a magnetic stirrer was used to dissolve 5 g of Ag₂NO₃ in 100 ml of deionized water for 60 minutes at 5000 rpm/min. Next, following our earlier research, a FeCl₃ solution was added to 100 millilitres of deionized water and exposed to PLA (Nd: YAG) radiation (Hajiali et al., 2024). After that, 100 ml of marine shrimp extract was

mixed with 200 ml of Ag_2NO_3 and Fe_2O_3 solutions. This colloid was irradiated with 200 Mj and 1500 pulses at 6 Hz. The distance between the laser gun and the sample is 5 cm. The $\text{AgO}/\text{Fe}_2\text{O}_3$ NCs colloidal solution was created in the same solution and then exposed to another round of laser radiation. For seventy minutes, the two solutions were combined using a magnetic stirrer. Deionized water was used to wash the precipitate many times. For three hours, the drying procedure was conducted in an oven set at 200°C . Experimental conditions such as laser parameters, reaction environment, and precursor concentrations are shown in Table 2.

Table 2

The experimental conditions used in this work.

Laser parameters		Reaction environment		Concentration	
Energy	200 Mj	Temperature	200°C	Ag_2NO_3	1M
Frequency	6 Hz	PH	7	FeCl_3	1M
Pulses	1500	Time	3 hours		
Distance	5 cm				

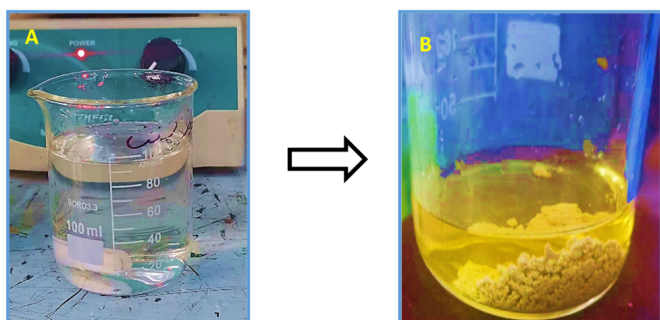


Figure 2. The synthesis stages of $\text{AgO}/\text{Fe}_2\text{O}_3$ NCs using the PLA (Nd-YAG) technique.

2.4. Characterization of $\text{AgO}/\text{Fe}_2\text{O}_3$ NCs synthesized by the PLA (Nd-YAG technique)

The Shimadzu-Japan XRD-6000 apparatus was utilized, and its measurement range was 10 to 80° . At 40 kV and 30 mA, the X-ray generator ran. The XRD instrument's scan range was used to compare the acquired diffraction patterns to the information supplied by the Joint Committee on Powder Diffraction Standards (JCPDS) card. The function groups are identified using the FTIR spectrum (Perkin-Elmer Spectrum GX FTIR). FTIR spectroscopy is an essential tool for determining a substance's molecular structure. A molecule's basic parts and bonding arrangement can be ascertained by examining the single resonant vibrational modes of its different branches or body regions. Since each molecule has a distinct infrared spectrograph that may be used to identify it, the opposite process is also employed, much like a fingerprint. Over the past ten years, FTIR spectroscopy analysis—a technique based on the concept of infrared spectroscopy—has found more use in researching materials at the nanoscale (Baudot et al., 2010). Using a FESEM device, Tuscan Mira3 FESEM-Czechia

in Mashhad, Iran, has evaluated the samples. One of the most commonly used methods for characterizing nanoparticles is FE-SEM with Energy Dispersive Spectrometry (EDS).

Because of their small size (1 – 100 nm), optical microscopes cannot detect them, necessitating such approaches. High-resolution imaging in FE-SEM enables the imaging of particles, while EDS provides elemental and chemical information on nanoparticles. (FE-SEM and TEM) offer essential insights into the size and shape of the generated nanoparticles (NPs). At various magnifications, the FE-SEM and TEM fields yielded microstructural and nanoscale data, such as particle size and morphological features, at a voltage of 20.00 KV. TEM was the most advanced and effective technology for imaging materials. However, the TEM tools could not handle the demands of photographing such one-nm-sized atom clusters due to insufficient spatial resolution. Feynman emphasized the need for improved spatial resolution in TEM equipment (Anjum, 2016).

2.5. Antimicrobial activity of $\text{AgO}/\text{Fe}_2\text{O}_3$ NCs prepared from marine shrimp shell extract by PLA (Nd-YAG) technique

The antimicrobial potential of the prepared samples ($\text{AgO}/\text{Fe}_2\text{O}_3$ -NCs) was investigated against gram-negative and gram-positive bacterial strains using an agar-well diffusion assay. About 20 mL of Muller-Hinton (MH) agar was aseptically poured into sterile Petri dishes via diffusion. The bacterial species were collected using a sterile wire loop from their stock cultures. After culturing the organisms, six mm-diameter wells were bored on the agar plates using a sterile tip. In the bored wells, 30 mg/L concentrations of the samples ($\text{AgO}/\text{Fe}_2\text{O}_3$ -NCs) worked. After being incubated at 37°C for the whole night, the test organisms and the $\text{AgO}/\text{Fe}_2\text{O}_3$ -NCs samples were placed on cultivated plates. The average diameter of the zones of inhibition was then measured and recorded. The University of Baghdad—College of Education for Pure Science (Ibn al-Haitham) microbiology lab supplied the microbial cultures. This test was conducted using sterile petri plates with a 90 -mm diameter that contained sterile nutritional agar medium using the agar-well diffusion technique. In 1000 millilitres of deionized water, 0.5 grams of peptone—which supplies organic nitrogen— 0.3 grams of yeast extract—which supplies vitamins, carbohydrates, nitrogen, and salts—and 28 grams of agar—which gives the combination solidity—were dissolved to create nutrient agar medium. At 27°C , the pH was corrected to 6.9 . After mixing these components and boiling them for around 15 minutes at 121°C to ensure they are well incorporated, the mixture is placed into petri dishes and covered immediately to solidify. Next, $\text{AgO}/\text{Fe}_2\text{O}_3$ -NCs were dissolved in a 30 mg/mL solution of dimethyl sulfate (DMSO) solvent. The Petri plate surface was swabbed with the recently created microorganisms. Using a sterile gel puncher or cork borer, 8 mm diameter wells were made in the medium containing bacterial and fungal life for every plate. For bacteria and fungi, 40 μL of $\text{AgO}/\text{Fe}_2\text{O}_3$ -NCs and DMSO control are present in each well at the appropriate concentration. The

test specimens were incubated for 24 hours at ± 25 °C to grow bacteria and fungus. The width of the inhibitory zone was then measured in millimetres. A bacterial culture dish was fertilized for AgO/Fe₂O₃-NCs by the PLA (Nd-YAG) technique, explaining the different levels of inhibition of zones in the dose-depending style. The AgO/Fe₂O₃-NCs intrinsically exhibit high levels of inhibition of zone versus gram-negative (*Escherichia coli*) and gram-positive (*Staphylococcus aureus*, *Staphylococcus epidermidis*). The following calculation has been used to calculate the percentage of the inhibition zone (Hajjali et al., 2024):

$$\text{Inhibition zone(\%)} = \frac{\text{Diameter of the inhibition zone in mm}}{\text{Diameter of particulate (90 mm)}} \times 100 \% (1)$$

3. RESULT AND DISCUSSION

3.1. XRD of AgO/Fe₂O₃ NCs prepared from marine shrimp shell extract by PLA (Nd-YAG technique)

The XRD pattern was used for the structure-properties study of AgO/Fe₂O₃ NCs prepared from the marine shrimp shell extract via the PLA (Nd-YAG) technique at 200 Mj with 1500 pulses. Figure 3 and Table 3 show good crystallinity and many diffraction peaks for AgO/Fe₂O₃ NCs. The crystal structure of AgO/Fe₂O₃ NCs is cubic-like and has been shown and matched with (00-087-1526). There are four more distinguished peaks below the AgO NCs at 32.1°, 46.6°, 67°, and 76.1° that correspond to (111), (200), (220), and (311), respectively. Fe₂O₃ nanoparticles produce overlapping diffraction angles with miller (012), (024), and (116) patterns. The crystallite size of AgO/Fe₂O₃ NCs is 9.6 to 19.5 nm. The formula developed by Debye Scherer was used to determine the crystallite size of AgO/Fe₂O₃ NCs (Abid et al., 2021; Abid & Kadhim, 2020):

$$\text{Crystallite size (D)} = \frac{0.9\lambda}{\beta \cos \theta}$$

Where λ is the wavelength of the X-ray = 1.5406 Å, β is the full-width half maximum (FWHM) of the peak in radians, and θ is the Bragg angle.

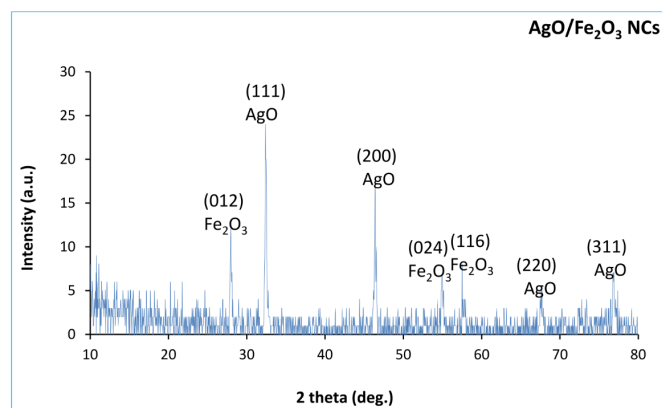


Figure 3. XRD pattern of AgO/Fe₂O₃ NCs preparation from shrimp marine extract by PLA (Nd-YAG) technique.

3.2. FE-SEM of AgO/Fe₂O₃ NCs prepared from marine shrimp shell extract by PLA (Nd-YAG technique)

The FE-SEM pictures at an accelerated voltage of 10 kV and a magnification of 50K are shown in Figure 4. AgO/Fe₂O₃-NCs have an irregular form, as shown in Figure 4(A), and their mean particle size is between 29 and 40 nm. These images display the apparent NP aggregation. Thermodynamics dictates that due to the high power of laser ablation, species collisions in relatively high-energy states should produce NPs soon at the beginning of ablation. In contrast, neutral species aggregations may be the source of nucleation. Figure 4 (B) illustrates how the AgO/Fe₂O₃-NCs assemble into multi-layered structures after longer ablation durations (Amrillah, 2022; Karpagavinayagam & Vedhi, 2019).

3.3. TEM of AgO/Fe₂O₃ NCs prepared from marine shrimp shell extract by the PLA (Nd-YAG) technique

To identify the morphology and the particle size of AgO/Fe₂O₃ NCs prepared from marine shrimp extract by PLA (Nd-YAG) technique via TEM device. TEM images show that AgO/Fe₂O₃ NCs are spherical and aggregated significantly, as shown in Figure 5A–B. The color of AgO/Fe₂O₃ NCs changed from white to lead dark when using marine shrimp shell extract.

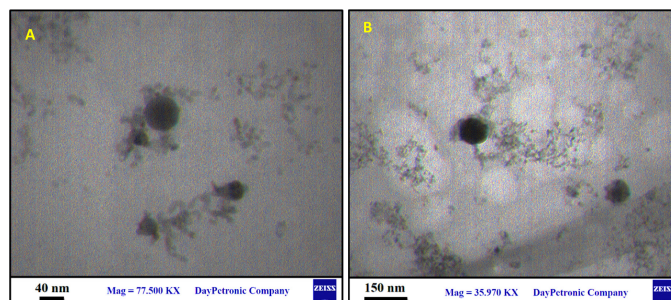


Figure 5. B): TEM images of AgO/Fe₂O₃ NCs prepared from the marine shrimp shell extract by PLA (Nd-YAG) technique.

3.4. EDS and mapping of AgO/Fe₂O₃ NCs prepared from marine shrimp shell extract by PLA (Nd-YAG) technique

AgO-Fe₂O₃ NCs' elemental composition was examined using EDS. Figure 6 and Table 4 illustrate that iron (Fe), oxygen (O), and silver (Ag) were the three prominent peaks. The many phytochemicals included in the extract were the primary cause of the signals for C, N, and K. The presence of an oxygen signal further confirms the creation of iron oxide nanoparticles. For Fe, O, and Ag, the weight percent (wt%) from nanoparticles was determined to be 16.33%, 28.33%, and 24.35%, respectively (Ali et al., 2021; Elbasuney et al., 2022). The as-prepared nanoparticles may be readily magnetically recovered due to the high Fe loading. It would result from the marine shrimp extract of the substance. The EDX elemental mapping of a single particle aggregate is shown in Figure 6B. The X-ray signals from Ag, Fe, and O are represented by blue,

Table 3

The diffraction angles, Miller indices, full width at half maximum (FWHM), and crystallite size for every diffraction angle.

Material	Phase	Angle 2θ (deg.)	FWHM β (deg.)	Angle 2θ (rad)	FWHM β (rad)	Crystallite size D(nm)	Dislocation density (δ)	Microstrain (ϵ)
Marine shrimp extract	AgO/Fe ₂ O ₃ NCs	28.9	0.59	0.25	0.0103	13.8	52.26	25.05
		32.0	0.64	0.28	0.0112	12.8	60.59	26.97
		46.0	0.89	0.40	0.0156	9.65	107.3	35.90
		55.7	0.69	0.48	0.0121	12.9	59.47	26.72
		56.4	0.46	0.49	0.0080	19.5	26.26	17.75
		57.2	0.59	0.50	0.0103	15.2	42.87	22.68
		68.0	0.76	0.59	0.0133	12.5	63.34	27.57
		77.3	0.87	0.67	0.0152	11.6	73.55	29.71

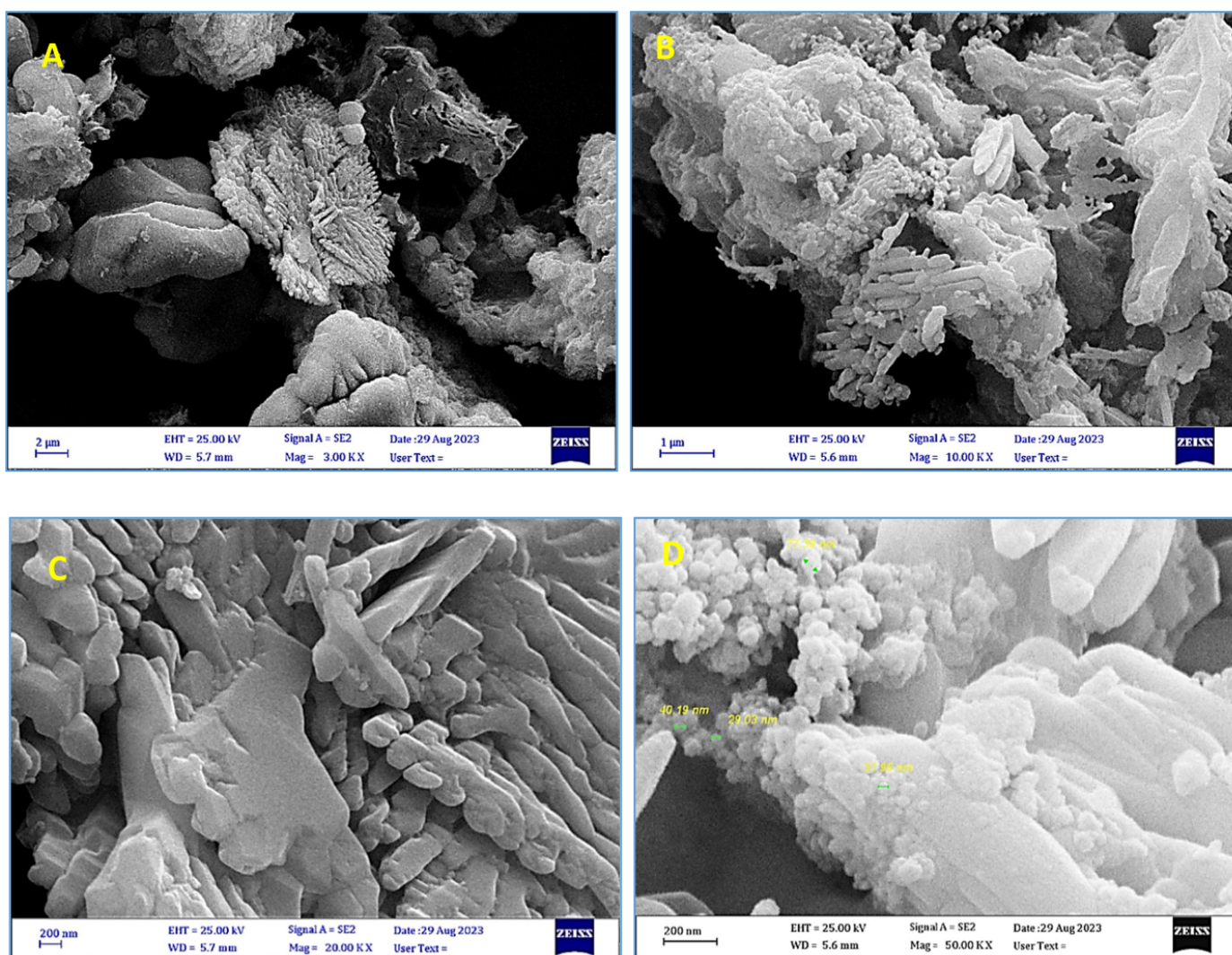


Figure 4. FE-SEM images of AgO/Fe₂O₃ NCs prepared from marine shrimp shell extract by PLA (Nd-YAG) technique.



Figure 6. Mapping and EDS images of AgO/Fe₂O₃ NCs preparation from the marine shrimp shell extract by PLA (Nd-YAG) technique.

green, and yellow, respectively. The collected data demonstrates that all of these components' spatial distribution inside the nanocomposite is relatively uniform (Kadhim et al., 2023; Salih et al., 2023).

Table 4

The elements, line type, weight, weight sigma, and atomic percentage of AgO/Fe₂O₃ NCs preparation from the marine shrimp shell extract by PLA (Nd-YAG) technique.

Element	Line Type	Weight %	Weight % Sigma	Atomic %
O	K series	28.33	0.58	34.83
Fe	K series	16.33	0.32	5.75
Cu	K series	7.85	0.20	2.43
K	K series	0.41	0.03	0.21
Ag	L series	0.78	0.09	0.14
Ag	K series	24.35	1.18	39.88
O	K series	16.55	0.31	9.18
Ag	K series	5.40	0.82	7.58

3.5. FTIR spectrum of AgO/Fe₂O₃ NCs prepared from marine shrimp shell extract by PLA (Nd-YAG) technique

The FTIR spectra of AgO/Fe₂O₃ NCs in the 4000-500 cm⁻¹ range are shown in Figure 7. The peaks at 3899.61, 3847.18, 3742.40, 3675.89, 3646.54, 3491.07, 3450.86, and 3413.63 cm⁻¹ correspond to the O-H stretching of the free OH group. An alkynes' C-H bond stretching vibrations are responsible for the 3063.64 cm⁻¹ peak. The peak at 2923.77 cm⁻¹ is caused by the amine salt's N-H bond stretching. A signal at 2854.52 cm⁻¹ represents asymmetric stretching vibrations of CH₂ in aliphatic hydrocarbons. A 2586.08 and 2367.49 cm⁻¹ peak are attributed to alkynes' C=C stretching vibrations. After phase transfer, a new band at 1843.88 cm⁻¹ develops. The carboxylic acid's C=O bond stretching vibrations are responsible for the 1742.41 cm⁻¹ peak. This corresponds to the symmetric vibration modes of the COO group, indicating chemical interactions between the carboxyl groups. The stretching vibration of an acyclic C-C produced from aromatic rings, shown by the strong peak at 1636.35 cm⁻¹ with 1523.83 and 1456.22, is present in marine shrimp

marine shell extract. To the amine group, 1393 cm⁻¹ and 1042 cm⁻¹ associated. Ag-O bending vibrations (fingerprint) had 785.44 and 821.47 cm⁻¹ peaks, while the Fe-O vibrations (fingerprint) had 785.13 and 726.46 cm⁻¹ peaks, as shown in Figure 7 (Batoo et al., 2024; Jasim et al., 2020; Kadhim et al., 2022; Satheesh et al., 2014).

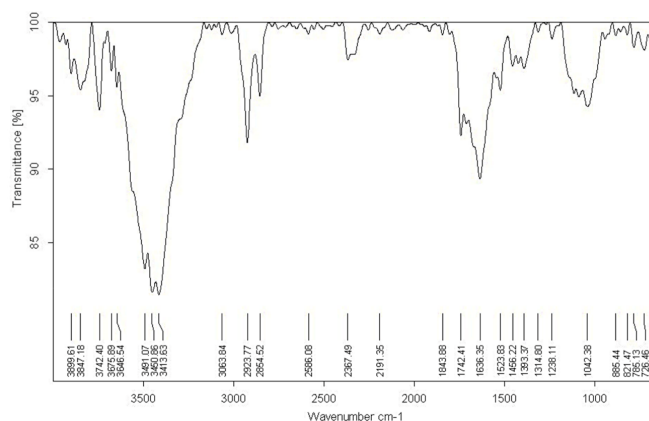


Figure 7. FTIR spectrum of AgO/Fe₂O₃ NCs prepared from marine shrimp shell extract by PLA (Nd-YAG) technique.

3.6. Antimicrobial activity of AgO/Fe₂O₃ NCs prepared from marine shrimp shell extract by PLA (Nd-YAG) technique

The AgO/Fe₂O₃ NCs made from marine shrimp shell extract using the PLA (Nd-YAG) approach showed antibacterial efficacy against both gram-positive (*Staphylococcus aureus*) and gram-negative (*Escherichia coli*) bacteria. The antibacterial activity of marine shrimp shell extract stabilizer-based AgO/Fe₂O₃-NCs was examined using the agar well diffusion method compared to bacteria (Aldahasi et al., 2024; Chircov et al., 2022; Dewangan et al., 2024; Ezealigo et al., 2021a; Ghazzy et al., 2024; Li et al., 2019). The inhibition zones of pathogenic gram-negative bacteria (*Escherichia coli*) and gram-positive bacteria (*Staphylococcus aureus* and *Staphylococcus epidermidis*) are displayed in Figure 8(A-C). One well-indicated via AgO/Fe₂O₃-NCs is loaded with 30 mg/L (AgO/Fe₂O₃-NCs) (Attia et al., 2022; Edwar et al., 2023; Ezealigo et al.,

2021b; Zhang et al., 2022). It determined the proportion of destroyed bacteria when AgO/Fe₂O₃-NCs were used with marine shrimp shell extract. This is because it was evident that the biomolecules in the chard extract had a more significant impact than the biomolecules in the shrimp extract, and the outcome was excellent and distinct from previous findings (Shaymaa, Ismail, Kadhim, et al., 2023).

The inhibition of zone (%) of AgO/Fe₂O₃-NCs using marine shrimp extract by a PLA (Nd-YAG) technique at 30 mg/L. With the applied PLA technique, when employing AgO/Fe₂O₃-NCs from marine shrimp shell extract, it was shown that the percentage of destruction for gram-positive and gram-negative bacteria was good. The results of the destruction of the three types of bacteria and a kind of fungi, as shown in Figure 8 and 9 and Table 5 (Ansari et al., 2023; Ejileugha et al., 2021; Homsı et al., 2023; Nzilu et al., 2023; Shah & Bharadvaja, 2024; Shaymaa, Ismail, Ali, et al., 2023). Because of their ultra-small, controlled size, AgO/Fe₂O₃ NCs are ideal for performing antibacterial operations and battling internal microorganisms. The nanocomposites' crystallite size, particle size, shape, elemental composition, and functional groups are so tiny that bacteria cells may readily phagocytose them. Furthermore, numerous NC kinds have structures that bacteria can use. (for example, liposomal NCs, whose walls are composed of one or more lipid bilayers surrounding sphere-shaped NCs), and the flexibility of NCs to enter host cells via endocytosis allows the majority of the nano to be released intracellularly (Wang et al., 2017).

The antifungal activity of *Candida* was used in the AgO/Fe₂O₃-NCs preparation of marine shrimp extract using the PLA (Nd-YAG) technique. The antifungal activity of AgO/Fe₂O₃-NCs from marine shrimp shell extract stabilizer-based was investigated versus *Candida albicans* by the agar well diffusion technique. It is observed that the effect of AgO/Fe₂O₃-NCs on *Candida* is high, as shown in Figure 8D (Abbas et al., 2024; Carrière & Larue, 2012; Ghelich et al., 2022; Kadhim et al., 2024; Prathap et al., 2023).

One of the leading causes of illness in both industrialized and poor countries is thought to be bacterial infection. The pathogens change throughout time, developing resistance to previously found antibiotics. Every year, two million individuals worldwide are afflicted with various types of bacteria, and 700,000 of them die as a result of bacterial resistance. For instance, in the US and Europe, *Staphylococcus aureus*, *Staphylococcus epidermidis*, and *Escherichia coli* are responsible for 50,000 deaths annually. Because of this, specialists are growing more worried about how well-suited contemporary antibiotics are to treating a range of infectious diseases. A lot of research was done on creating new, alternative drugs to treat resistance problems. Nature is a possible source for drug discovery. The biological components and phytochemicals found in plants have long piqued the interest of scientists due to their various structures, low toxicity, and increased human acceptability. There are several of these antimicrobial phytochemicals (Jubair et al., 2021).

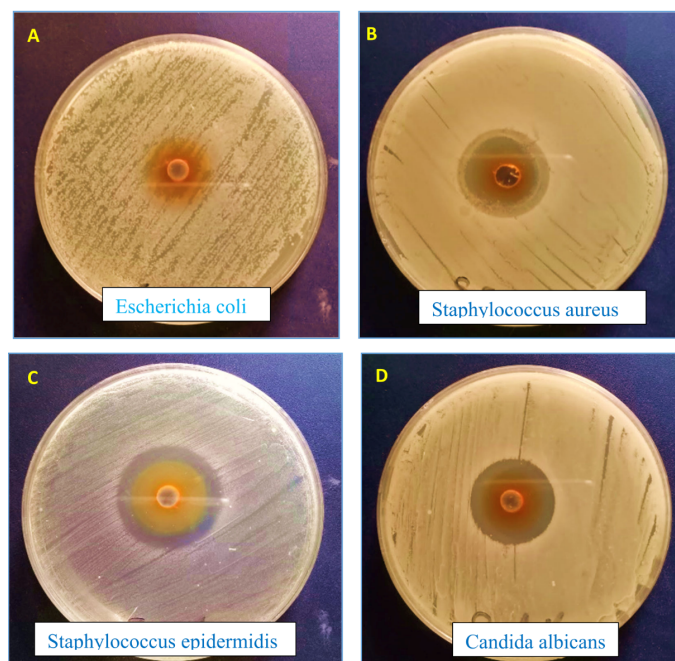


Figure 8. Depicts the antimicrobial activity of AgO/Fe₂O₃ NCs prepared from marine shrimp shell extract by the PLA (Nd-YAG) technique, A) *Escherichia coli* bacteria, B) *Staphylococcus aureus* bacteria, C) *Staphylococcus epidermidis*, and D) *Candida albicans*.

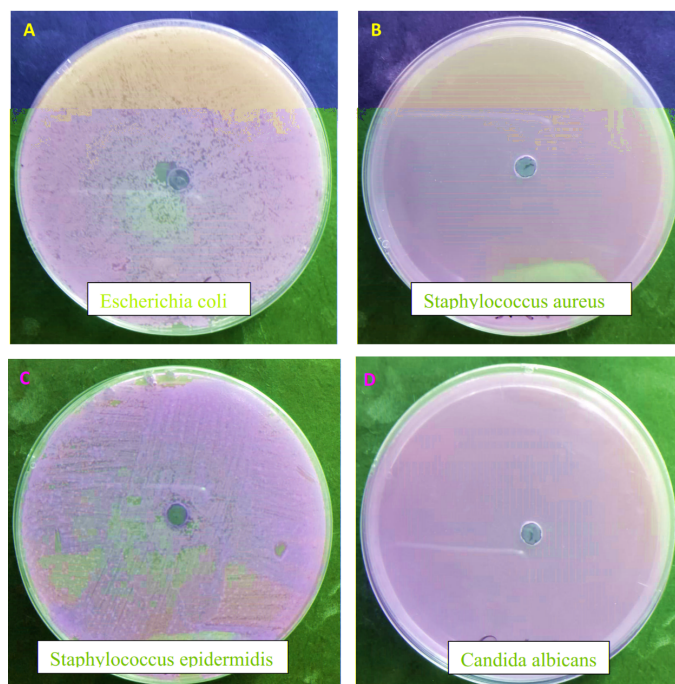


Figure 9. D) depicts the antimicrobial activity of control (D. W.), A) *Escherichia coli* bacteria, B) *Staphylococcus aureus* bacteria, C) *Staphylococcus epidermidis*, and D) *Candida albicans*.

Table 5Results of the antimicrobial activity of AgO/Fe₂O₃ NCs prepared from marine shrimp shell extract by PLA (Nd-YAG) technique.

Extract	Material	Gram-negative (-)	Gram-positive (+)		Antifungal	Percentage of inhibition zone (%)			
		<i>E. coli</i>	<i>S. aureus</i>	<i>S. epidermidis</i>	<i>Candida albicans</i>	<i>E. coli</i>	<i>S. aureus</i>	<i>S. epidermidis</i>	<i>Candida albicans</i>
Marine shrimp shell extract	AgO/Fe ₂ O ₃	40 mm	29 mm	13.5 mm	42 mm	45.5 mm	34 mm	17.5 mm	45 mm
Control	D.W.	0	0	0	0	0	0	0	0

4. CONCLUSION

This research developed a natural resource marine shrimp shell extract for synthesising AgO/Fe₂O₃-NCs by the PLA (Nd-YAG) technique at 1500 pulses and 200 Mj. As revealed by XRD analysis, AgO/Fe₂O₃-NCs have crystallite sizes ranging from 9.6 to 19.5 nm. AgO/Fe₂O₃-NCs had a particle size and shape of around 10 nm, and FE-SEM examination revealed that the particles had a nano-spherical structure. The AgO/Fe₂O₃-NCs properties have excellent behavior toward anti-negative, anti-positive bacterial, and antifungal activity. TEM scans indicated that AgO/Fe₂O₃ NCs were spherical and aggregation-shaped, with sizes ranging from 15.4 to 23 nm. Using EDS analysis, the elemental values of AgO/Fe₂O₃-NCs were found to be 16.33%, 28.33%, and 24.35%, respectively. According to the FTIR spectra, the prominent absorption peaks of AgO/Fe₂O₃-NCs are 726 cm⁻¹. AgO/Fe₂O₃-NCs EDS mapping results show that the spatial distribution of all these components inside the NCs is relatively uniform. Relative to AgO/Fe₂O₃-NCs, they exhibited the best response to high killing for antibacterial. The inhibition zones of antibacterial agents utilizing AgO/Fe₂O₃ NCs were determined using the diffusion technique. The inhibition zones measured 29 to 13.5 mm for gram-positive bacteria (*Staphylococcus aureus* and *Staphylococcus epidermidis*) and 40 mm for gram-negative bacteria (*Escherichia coli*); *Candida* had an inhibition zone diameter (IZD) of 42 mm. The nanocomposite used against bacteria and fungi was the mechanism of effect of the properties. To enhance the inhibitory zone region, the following antibacterial and antifungal characteristics must be changed and improved: Average grain size: When particles are lowered to the nanoscale, their specific surface area and the number of active sites rise.

CONFLICTS OF INTEREST

The authors declare that they have no known competing financial interests or personal relationships that could have appeared to influence the work reported in this paper.

ACKNOWLEDGMENTS

The author (s) would like to thank Mustansiriyah University (www.uomustansiriyah.edu.iq) Baghdad-Iraq for its support in the present work.

ORCID

Duha A. Kadhim	0009-0003-7012-5968
Abdul Haleem A. Raheem	0009-0009-9159-0723
Nada Qasim	0009-0008-0421-8601
Muslim A. Abid	0000-0002-8158-3388
Ihab Adnan Thabet	0000-0003-4465-7592

AUTHOR CONTRIBUTIONS

The authors confirm contribution to the paper as follows: study conception and design: Duha A. Kadhim; data collection: Abdul Haleem A. Raheem; analysis and interpretation of results: Nada Qasim; supervisor: Muslim A. Abid; draft manuscript preparation: Ihab Adnan Thabet. All authors reviewed the results and approved the final version of the manuscript.

REFERENCES

- Abbas, H.M., Gdoura, R., Al-Marjani, M.F., 2024. Unveiling the High Prevalence of Antibiotic Resistance and Quorum Sensing Genes in Uropathogenic *Escherichia coli*. *Al-Mustansiriyah Journal of Science*. 35(1), 38–43. <https://doi.org/10.23851/mjs.v35i1.1429>
- Abid, M.A., Abid, D.A., Aziz, W.J., Rashid, T.M., 2021. Iron oxide nanoparticles synthesized using garlic and onion peel extracts rapidly degrade methylene blue dye. *Physica B: Condensed Matter*. 622, 413277. <https://doi.org/10.1016/j.physb.2021.413277>
- Abid, M.A., Kadhim, D.A., 2020. Novel comparison of iron oxide nanoparticle preparation by mixing iron chloride with henna leaf extract with and without applied pulsed laser ablation for methylene blue degradation. *Journal of Environmental Chemical Engineering*. 8(5), 104138. <https://doi.org/10.1016/j.jece.2020.104138>
- Aldahasi, R.M., Shami, A., Mohammed, A.E., 2024. Bimetallic nanoparticles and biochar produced by *Adansonia Digitata* shell and their effect against tomato pathogenic fungi. *PeerJ*. 12, e17023. <https://doi.org/10.7717/peerj.17023>
- Ali, S.M., Hussein, E.H., Dakhil, O.A.A., 2021. Photocatalytic activity of ZnO/NiO nano-heterojunction synthesized by modified-chemical bath deposition. *Nano Futures*. 5(3), 35001–35001. <https://doi.org/10.1088/2399-1984/ac1dba>
- Amrillah, T., 2022. All Shapes and Phases of Nanometer-Sized Iron Oxides Made from Natural Sources and Waste Material via Green Synthesis Approach: A Review. *Crystal Growth & Design*. 22(7), 4640–4660. <https://doi.org/10.1021/acs.cgd.2c00485>
- Anjum, D.H., 2016. Characterization of nanomaterials with transmission electron microscopy. *IOP Conference Series: Materials Science and*

- Engineering. 146, 12001. <https://doi.org/10.1088/1757-899X/146/1/012001>
- Ansari, P.M.Y., Muthukrishnan, R.M., Khan, R.I., Vedhi, C., Sakthipandi, K., Kader, S.A., 2023. Green synthesis of copper oxide nanoparticles using *Amaranthus dubius* leaf extract for sensor and photocatalytic applications. *Chemical Physics Impact*. 7, 100374. <https://doi.org/10.1016/j.chphi.2023.100374>
- Attia, N.F., El-Monaem, A., El-Aqapa, E.M., Elashery, H.G., Eltaweil, S.E., Kady, A.S.E., M, El-Seedi, .., R, H., 2022. Iron oxide nanoparticles and their pharmaceutical applications. *Applied Surface Science Advances*. 11, 100284. <https://doi.org/10.1016/j.apsadv.2022.100284>
- Batoo, K.M., Abid, M.K., Hamoody, A.H.M., Alkadir, O.K.A., Hussain, S., Alawadi, A., Alsalamy, A., 2024. Magnetic nanomaterials as green and recoverable nanocatalysts: Research on synthesis of benzimidazole derivatives, 1–26. <https://doi.org/10.1080/00397911.2024.2325786>
- Baudot, C., Tan, C.M., Kong, J.C., 2010. FTIR spectroscopy as a tool for nanomaterial characterization. *Infrared Physics & Technology*. 53(6), 434–438. <https://doi.org/10.1016/j.infrared.2010.09.002>
- Betty, C.A., Choudhury, S., Shah, A., 2022. Nanostructured metal oxide semiconductors and composites for reliable trace gas sensing at room temperature. *Surfaces and Interfaces*. 36, 102560. <https://doi.org/10.1016/j.surfin.2022.102560>
- Carrière, M., Larue, C., 2012. Ecotoxicity of Inorganic Nanoparticles: From Unicellular Organisms to Invertebrates, B. Bhushan et al., (Eds.), *Encyclopedia of Nanotechnology*. Springer, Dordrecht, pp. 623–636. https://doi.org/10.1007/978-90-481-9751-4_332
- Chircov, C., Ștefan, R.E., Dolete, G., Andrei, A., Holban, A.M., Oprea, O.C., Tihăuan, B., 2022. Dextran-coated iron oxide nanoparticles loaded with curcumin for antimicrobial therapies. *Pharmaceutics*. 14(5), 1057. <https://doi.org/10.3390/pharmaceutics14051057>
- De Jesus, R.A., De Assis, G.C., De Oliveira, R.J., Costa, J.A.S., Silva, C.M.P.D., Iqbal, H.M., Ferreira, L.F.R., 2024. Metal/metal oxide nanoparticles: A revolution in the biosynthesis and medical applications. *Nano-Structures & Nano-Objects*. 37, 101071–101071. <https://doi.org/10.1016/j.nanoso.2023.101071>
- Dewangan, S., Bhatia, A.K., Singh, A.K., Carabineiro, S.A., 2024. Magnetic polymeric and silver nanocomposites: Properties, synthesis, and antimicrobial evaluation. *Magnetic Nanoparticles and Polymer Nanocomposites*, 17–35. <https://doi.org/10.1016/B978-0-323-85748-2.00002-5>
- Edwar, D.A., Naji, E.N., Maleki, A., 2023. Biofilm And Hemolysis Profile Index in Bacteria Isolated from Pre-Cesarean Surgery and Post Cesarean Infections. *Al-Mustansiriyah Journal of Science*. 34(4), 8–18. <https://doi.org/10.23851/mjs.v34i4.1341>
- Ejileugha, C., Ezealisiji, K.M., Ezejiofor, A.N., Orisakwe, O.E., 2021. Microbiologically influenced corrosion: uncovering mechanisms and discovering inhibitor-metal and metal oxide nanoparticles as promising biocorrosion inhibitors. *Journal of Bio-and Tribo-Corrosion*. 7(3), 109. <https://doi.org/10.1007/s40735-021-00545-0>
- Elbasuney, S., El-Sayyad, G.S., Attia, M.S., Abdelaziz, A.M., 2022. Ferric oxide colloid: Towards green nano-fertilizer for tomato plant with enhanced vegetative growth and immune response against fusarium wilt disease. *Journal of Inorganic and Organometallic Polymers and Materials*. 32(11), 4270–4283. <https://doi.org/10.1007/s10904-022-02442-6>
- Ezealigo, U.S., Ezealigo, B.N., Aisida, S.O., Ezema, F.I., 2021a. Iron oxide nanoparticles in biological systems: Antibacterial and toxicology perspective. *JCIS Open*. 4, 100027. <https://doi.org/10.1016/j.jciso.2021.100027>
- Ezealigo, U.S., Ezealigo, B.N., Aisida, S.O., Ezema, F.I., 2021b. Iron oxide nanoparticles in biological systems: Antibacterial and toxicology perspective. *JCIS Open*. 4, 100027. <https://doi.org/10.1016/j.jciso.2021.100027>
- Galúcio, J.M., De Souza, S.G.B., Vasconcelos, A.A., Lima, A.K.O., Costa, K.S.D., Braga, H.D.C., Taube, P.S., 2022. Synthesis, characterization, applications, and toxicity of green synthesized nanoparticles. *Current Pharmaceutical Biotechnology*. 23(3), 420–443. <https://doi.org/10.2174/1389201022666210521102307>
- Ghazzy, A., Nsairat, H., Said, R., Sibai, O.A., Aburuman, A., Shraim, A.S., 2024. Magnetic iron oxide-based nanozymes: from synthesis to application. *Nanoscale Advances*. 6, 1611–1642. <https://doi.org/10.1039/D3NA00903C>
- Ghelich, P., Kazemzadeh-Narbat, M., Najafabadi, A.H., Samandari, M., Memić, A., Tamayol, A., 2022. (Bio) manufactured Solutions for Treatment of Bone Defects with an Emphasis on US-FDA Regulatory Science Perspective. *Advanced nanobiomed research*. 2(4), 2100073. <https://doi.org/10.1002/anbr.202100073>
- Hajjali, S., Daneshjou, S., Daneshjoo, S., Khajeh, K., 2024. Biosynthesis Optimization of Antibacterial-Magnetic Iron Oxide Nanoparticles from *Bacillus megaterium*. *Biological Trace Element Research*, 1–18. <https://doi.org/10.1007/s12011-024-04168-7>
- Homsy, A., Al-Said, W., Tahan, Z., 2023. Detection of Some Virulence Genes in Diarrheagenic *Escherichia Coli* Pathotypes in Children Under Five Years in Aleppo City. *Al-Mustansiriyah Journal of Science*. 34(4), 19–28. <https://doi.org/10.23851/mjs.v34i4.1359>
- Islam, M.R., Akter, T., Hossain, A., Tora, A.T., Mely, S.S., Hossain, M.A., Haque, M.M., 2024. Contribution and prospect of marine fisheries in the economy of Bangladesh and sustainable blue economy challenges: A review. *Marine Science and Technology Bulletin*. 13(1), 41–55. <https://doi.org/10.33714/masteb.1337034>
- Jasim, M.M., Dakhil, O.A.A., Hussein, E.H., Abdullah, H.I., 2020. Enhanced photoelectrochemical properties of NiO nanoparticles-decorated TiO₂ nanotube arrays for water splitting. *Journal of Materials Science: Materials in Electronics*. 31, 10707–10714. <https://doi.org/10.1007/s10854-020-03620-3>
- Jubair, N., Rajagopal, M., Chinnappan, S., Abdullah, N.B., Fatima, A., 2021. Review on the antibacterial mechanism of plant-derived compounds against multidrug-resistant bacteria (MDR). *Evidenc. Evidence-Based Complementary and Alternative Medicine*. 2021, 3663315.
- Kadhim, D.A., Abid, M.A., Abdulghany, Z.S., Alhateem, J.Y., Kadhim, S.A., Aziz, W.J., Al-Marjani, M.F., 2022. Iron oxide nanoparticles synthesized using plant (*Beta vulgaris* and *Punica granatum*) extracts for a breast cancer cell line (MCF-7) cytotoxic assay. *Materials Technology*. 37(13), 2436–2444. <https://doi.org/10.1080/10667857.2022.2038766>
- Kadhim, D.A., Abid, M.A., Latif, L.A., Salih, W.M., Al-Kazazz, F.F., 2024. Blood-liquid extract inhibits bacteria through diffusion-mediated nano-CuO. *Nano-Structures & Nano-Objects*. 37, 101105. <https://doi.org/10.1016/j.nanoso.2024.101105>
- Kadhim, D.A., Abid, M.A., Salih, W.M., 2023. Study the degradation and photocatalytic activity of the methylene blue dye by mixing the Aloe vera extract with rust iron oxide nanoparticle. *Natural Resources for Human Health*. 3(3), 355–363. <https://doi.org/10.53365/nrfhh/170025>
- Karpagavinayagam, P., Vedhi, C., 2019. Green Synthesis of Iron Oxide Nanoparticles Using *Avicennia Marina* Flower Extract. *Vacuum*. 160, 286–292. <https://doi.org/10.1016/j.vacuum.2018.11.043>
- Khan, I., Saeed, K., Khan, I., 2019. Nanoparticles: Properties, applications and toxicities. *Arabian Journal of Chemistry*. 12(7), 908–931. <https://doi.org/10.1016/j.arabjc.2017.05.011>
- Khan, W.S., Hamadneh, N.N., Khan, W.A., 2016. Polymer

- nanocomposites-synthesis techniques, classification and properties. , and others, (Eds.), Science and applications of Tailored Nanostructures., pp. 50–50.
- Kumar, R., Kumari, N., Sahoo, G.C., 2024. Iron Oxide-Based Nanoparticles in Modern Antimicrobial and Antiviral Applications, Nanoparticles in Modern Antimicrobial and Antiviral Applications. Springer International Publishing, pp. 289–303. https://doi.org/10.1007/978-3-031-50093-0_13
- Li, D., Yan, X., Yang, M., Luo, C., Li, P., Hu, J., Li, G., Jiang, H., Zhang, W., 2019. 4-Mercaptobenzoic acid assisted synthesis of Au-decorated α - nanoparticles with highly enhanced photocatalytic performance. Journal of Alloys and Compounds. 775, 150–157. <https://doi.org/10.1016/j.jallcom.2018.10.073>
- López-Saiz, C.M., Suárez-Jiménez, G.M., Plascencia-Jatomea, M., Burgos-Hernández, A., 2013. Shrimp lipids: A source of cancer chemopreventive compounds. Marine drugs. 11(10), 3926–3950. <https://doi.org/10.3390/md11103926>
- Luceri, A., Francese, R., Lembo, D., Ferraris, M., Balagna, C., 2023. Silver nanoparticles: review of antiviral properties, mechanism of action and applications. Microorganisms. 11(3), 629. <https://doi.org/10.3390/microorganisms11030629>
- Mercan, D.A., Niculescu, A.G., Grumezescu, A.M., 2022. Nanoparticles for antimicrobial agents delivery-An up-to-date review. International Journal of Molecular Sciences. 23(22), 13862. <https://doi.org/10.3390/ijms232213862>
- Nasiri, K., 2023. Synthesis of Ag-Fe₂O₃ nanoparticles with Antibacterial and antifungal impacts on dental microbia. Nanomedicine Research Journal. 8(3), 283–289. <https://doi.org/10.22034/nmrj.2023.03.007>
- Nzilu, D.M., Madivoli, E.S., Makhanu, D.S., Wanakai, S.I., Kiprono, G.K., Kareru, P.G., 2023. Green synthesis of copper oxide nanoparticles and its efficiency in degradation of rifampicin antibiotic. Scientific Reports. 13(1), 14030. <https://doi.org/10.1038/s41598-023-41119-z>
- Prabhu, S., Poulouse, E.K., 2012. Silver nanoparticles: mechanism of antimicrobial action, synthesis, medical applications, and toxicity effects. International Nano Letters. 2, 1–10. <https://doi.org/10.1186/2228-5326-2-32>
- Prathap, N., Dravid, N., Kaarmukhnilavan, S.R., Shivakumar, M.S., Venkatesan, S., Shaik, M.R., Shaik, B., 2023. Copper Oxide Nanoparticles Synthesized from *Indigofera linnaei* Ali and This Plant's Biological Applications. Inorganics. 11(12), 1227–1249. <https://doi.org/10.3390/inorganics11120462>
- Salih, W.M., Sabah, R., Kadhim, D.A., Kadhum, H.A., Abid, M.A., 2023. Green synthesis of (CeO₂)-(CuO) nanocomposite, analytical study, and investigation of their anticancer activity against Saos-2 osteosarcoma cell lines. Inorganic Chemistry Communications, 111730. <https://doi.org/10.1016/j.inoche.2023.111730>
- Satheesh, R., Vignesh, K., Suganthi, A., Rajarajan, M., 2014. Visible light responsive photocatalytic applications of transition metal (M=Cu, Ni and Co) doped α -IO nanoparticles. Journal of Environmental Chemical Engineering. 2(4), 1956–1968. <https://doi.org/10.1016/j.jece.2014.08.016>
- Shah, M.P., Bharadvaja, N., 2024. Biogenic Nanomaterials for Environmental Sustainability: Principles, Practices, and Opportunities, Kumar L., (Eds.). Springer Cham, Switzerland, p. 508. <https://doi.org/10.1007/978-3-031-45956-6>
- Sharmin, S., Rahaman, M.M., Sarkar, C., Atolani, O., Islam, M.T., Adeyemi, O.S., 2021. Nanoparticles as antimicrobial and antiviral agents: A literature-based perspective study. Heliyon. 7(3), e06456. <https://doi.org/10.1016/j.heliyon.2021.e06456>
- Shaymaa, N., Ismail, E.M., Ali, A.M., Hussien, M.A.A., Alheety, 2023. Green synthesis and characterization of CdO nanoparticles from *Crocus sativus*: A promising material for hydrogen gas storage. Energy Storage. 2023, e534. <https://doi.org/10.1002/est2.534>
- Shaymaa, N., Ismail, J., Kadhim, Ban, A., Yousif, 2023. Iron oxide nanoparticles synthesized from mixing iron (iii) nitrate salt (Fe₂NO₃) with (curcumin) herbs extract for antibacterial activity. Journal of Survey in Fisheries Sciences. 10(3S), 1455–1464. <https://doi.org/10.17762/sfs.v10i3S.583>
- USDA., 2020. The Dietary Guidelines for Americans (Dietary Guidelines) . <https://health.gov/our-work/nutrition-physical-activity/dietary-guidelines>
- USEPA., n.d.. Health Effects of Exposures to Mercury. <https://www.epa.gov/mercury/health-effects-exposures-mercury>
- Wang, L., Hu, C., Shao, L., 2017. The antimicrobial activity of nanoparticles: present situation and prospects for the future. International journal of nanomedicine, 1227–1249. <https://doi.org/10.2147/IJN.S121956>
- Yamada, Y., Seno, Y., Masuoka, Y., Yamashita, K., 1998. Nitrogen oxides sensing characteristics of Zn₂SnO₄ thin film. Sensors and Actuators B: Chemical. 49(3), 248–252. [https://doi.org/10.1016/S0925-4005\(98\)00135-X](https://doi.org/10.1016/S0925-4005(98)00135-X)
- Zhang, S., Lin, L., Huang, X., Lu, Y.G., Zheng, D.L., Feng, Y., 2022. Antimicrobial properties of metal nanoparticles and their oxide materials and their applications in oral biology. Journal of Nanomaterials. 2022, 2063265. <https://doi.org/10.1155/2022/2063265>